Advanced Composites and Hybrid Materials (2023) 6:48
https://doi.org/10.1007/s42114-022-00622-z

RESEARCH

Creating poly(lactic acid)/carbon nanotubes/carbon black nanocomposites with high electrical conductivity and good mechanical properties by constructing a segregated double network with a low content of hybrid nanofiller

Tairong Kuang[1] · Maolin Zhang[1] · Feng Chen[1] · Yanpei Fei[1] · Jintao Yang[1] · Mingqiang Zhong[1] · Bozhen Wu[1] · Tong Liu[1]

Received: 29 October 2022 / Revised: 22 December 2022 / Accepted: 31 December 2022 / Published online: 26 January 2023

Abstract
Conductive biodegradable polymer composites have broad application prospects, but obtaining composites with high electrical conductivity and good mechanical properties at low filler content has been an important challenge. In this work, we melt blended poly(lactic acid) (PLA) and one-dimensional (1D) carbon nanotubes (CNTs) and found that CNTs can form part of the conductive network in the polymer matrix to improve its electrical conductivity. However, to achieve high electrical conductivity, PLA should be mixed with large amounts of CNTs, which inevitably impairs its mechanical properties. When carbon black (CB) was mechanically mixed with PLA/CNTs particles with sizes less than 200 μm, it not only formed a conductive network structure by itself but also interconnected with the CNTs network within the PLA/CNTs composites. Ultimately, a segregated double filler (0D CB–1D CNTs) network structure was constructed in PLA nanocomposites. The resulting nanocomposites achieved good electrical conductivity, tensile strength, flexural strength, and impact toughness of 9.8×10^{-2} S/m, 70.1 MPa, 91.3 MPa, and 2.8 kJ/m^2 at the addition of 1 *phr* CNTs and 1 *phr* CB, respectively. These results demonstrate that PLA-based composites with high electrical conductivity and good mechanical properties could be prepared using this technique at low filler content. This extends the application scope of PLA composites.

Keywords PLA nanocomposites · 0D CB–1D CNTs · Segregated double network · High electrical conductivity · Good mechanical properties

1 Introduction

The increasing discharge of electronic waste, including plastic waste, from discarded portable electronic and electrical equipment, has created a global environmental problem [1]. The e-waste problem is aggravated by the relatively short life expectancy of electronic equipment. Biodegradable polymeric materials are considered a viable alternative to non-degradable plastics [2–5]. Poly(lactic acid) (PLA), one of the most commonly used biodegradable polymeric materials, is a non-toxic and environmentally friendly polymer with high strength and excellent processability, biocompatibility, and biodegradability [6–9]. In recent years, many studies have investigated for preparing highly conductive PLA-based composites for electrical and electronic applications [10–15]. To improve their electrical conductivity, highly conductive fillers, such as metallic fillers and carbonaceous nanofillers, are incorporated into PLA composites to form a continuous conductive network skeleton in the PLA matrix [16–18]. Compared with other conductive fillers, carbonaceous nanofillers (e.g., one-dimensional (1D) fillers-carbon nanotubes (CNTs), two-dimensional (2D) fillers-graphene, and zero-dimensional (0D) fillers-carbon black (CB)) have been increasingly applied in conductive polymer composites because of their wide availability, lightweight,

✉ Tairong Kuang
kuangtr@zjut.edu.cn

✉ Bozhen Wu
wubz_314@163.com

✉ Tong Liu
liut@zjut.edu.cn

[1] College of Material Science and Engineering, Zhejiang University of Technology, Hangzhou 310014, China

low cost, as well as excellent electrical and mechanical properties [19–21].

Numerous studies have demonstrated that direct melt blending of PLA and carbonaceous nanofillers is an economical and efficient method of preparation biodegradable PLA composites [22–26]. More recently, Guo et al. [23] prepared PLA/CB composites with an electrical conductivity of 14 S/m by melt blending it with 16 wt% CB. However, addition of a large amount of CB filler resulted in a significant decrease in the tensile strength of the composites. Usually, to prepare homogeneous composite systems, a high amount of nanofillers is used to lap the conductive fillers together to form a complete conductive network. This method not only increases cost but also causes a significant decrease in the mechanical properties of the composites due to the high content of nanofillers, making them prone to agglomeration. Researchers have explored methods for improving the dispersion of carbon nanofillers to resolve the problem of high-filler content and find a balance between mechanical performance, electrical conductivity, and the cost of conductive polymer composites. Urquijo et al. [26] incorporated CNTs into PLA/poly(butyleneadipate-co-terephthalate) (PBAT) blends and found that CNTs could selectively disperse within the PBAT matrix. At a PLA to a PBAT ratio of 6:4, PLA/PBAT/CNTs composites exhibited electrical conductivity of 1.0×10^{-5} S/m at lower loadings (2 wt%) of CNTs. These results suggest that a more complete conductive network can be achieved with the same total filling content by constructing co-continuous structures in two immiscible polymer blends and dispersing the conductive filler selectively. A vital feature of this approach is the filler enrichment created by structural design to increase the polymer's electrical conductivity at a lower filler content. Another common strategy for filler enrichment distribution involves the creation of a segregated network structure between polymer and filler, i.e., adhering conductive filler to the surface of the polymer particles to improve conductivity at lower filler content. For example, Wang et al. [25] coated PLA particles with CNTs and graphene nanoplates (GNPs) using poly(ethylene oxide) (PEO) as a binder and hot pressed them to form PLA nanocomposites. They found that composites with a segregated structure had a higher electrical conductivity than composites with randomly distributed fillers. Notably, the formation of continuous segregated conductive networks in the polymer matrix was influenced by filler content and distribution method as well as the morphological structure of the filler. A segregated ultra-high molecular weight polyethylene (UHMWPE)/CNTs/CB composite containing different dimensions of carbon nanofillers was successfully prepared by Cui et al. With CNTs and CB contents of 3 wt% and 1 wt%, respectively, the hybrid CNTs/CB filler combines the advantages of both fillers over a single filler. Its electrical conductivity can reach 3.32 S/m, which is 14 times higher than that of pure UHMWPE. In this study, the CBs built independent conductive pathways and connected unconnected conductive CNTs, creating a better synergistic effect by adding more CB fillers. Of note, over-enrichment of filler on the segregated network resulted in weaker bonding between the polymer particles, decreasing the composite's mechanical properties. Thus, an effective method to prevent performance defects associated with excessively enriched fillers in the segregated structure of PLA composites is required to maximize the synergy between multiple fillers [27].

In the present study, we successfully constructed a continuously segregated double-filler network structure in PLA composites with improved electrical conductivity by adding small amounts of 1D CNTs and 0D CB hybrid fillers [5]. A masterbatch of PLA/CNTs composites with a continuous conductive network of CNTs was first obtained by melt blending. Then, by mechanically mixing a small amount of CB filler over the surface of the PLA/CNTs masterbatch, a thin layer of the segregated conductive network was formed. Analysis of electrical conductivity and mechanical properties showed that the PLA composites with the addition of 1 *phr* (parts per hundred of PLA) CNTs and 1 *phr* CB could maintain tensile strength of 70.1 MPa, impact toughness of 2.8 kJ/m^2, and flexural strength of 91.3 MPa, while their electrical conductivity could reach 9.8×10^{-2} S/m. Thus, the PLA composites prepared in this study exhibited excellent electrical conductivity and mechanical properties at low addition of nanofillers, demonstrating their broad application prospects in electronic components and safety protection.

2 Experimental section

2.1 Materials

PLA, grade 4032D, was obtained from Nature Works Co., Ltd (USA). Multi-walled carbon nanotubes (CNTs) were purchased from Nanjing XFNANO Technology Co., Ltd. (China) (purity > 95%, diameter and length of 10–20 nm and 10–30 μm, true density of 2.1 g/cm^3). Conductive carbon black (CB) (particle size of 30–45 nm) was also supplied by Nanjing XFNANO Technology Co., Ltd. (China).

2.2 Preparation of PLA/CNTs@CB composites with segregated double network structure

Figure 1 illustrates the schematic diagram of the preparation processes for PLA/CNTs@CB composites (PLA/*x*C@*y*B, where *x* and *y* denote CNTs and CB parts per hundred of PLA, respectively). All raw materials were dried in an oven at 70 °C for 8 h before composite preparation. To prepare composites, PLA pellets and CNTs were first melt blended in a Harker torque rheometer at a temperature of 180 °C and a speed of 60 r/

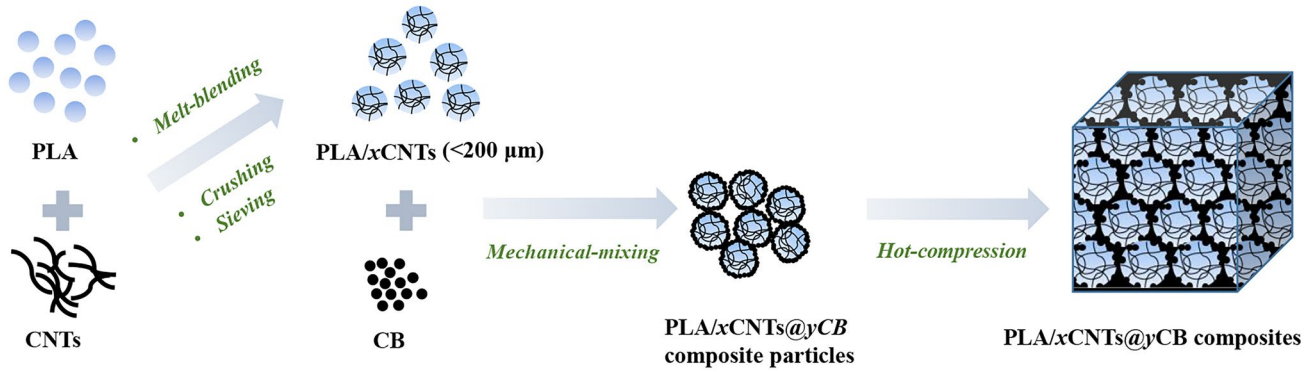

Fig. 1 The schematic diagram for the preparation procedures of the PLA/CNTs@CB composites

min for 8 min. The blended PLA/CNTs mixtures were then crushed at 30,000 r/min for 1.5 min and sieved to obtain PLA/*x*C powder masterbatches with sizes less than 200 μm. The PLA/*x*C powder masterbatch and the CB filler were mechanically mixed in a high-speed mixer at 28,000 r/min for 6 min to create PLA/*x*C@*y*B composite particles. Finally, PLA/*x*C@*y*B composite sheets were prepared by compression molding of composite particles at 190 °C and 10 MPa.

2.3 Electrical conductivity measurements

The volume conductivities for samples with a diameter of 25 mm and a thickness of 1 mm were measured using a four-point probe instrument (RTS-9, China) and a high-resistance meter (ZC36, China). Data reported were computed from the average conductivity of five repeated measurements at different locations, which were then converted to the average conductivity.

2.4 Rheological properties

Rheological properties were measured using a physical rheometer (Anton Paar MCR302, Austria) with a sample of 25 mm in a diameter and 1 mm in thickness. Rheological measurement was conducted at 190 °C from 0.1 to 100 rad/s with a strain amplitude of 1%.

2.5 Scanning electron microscopy (SEM)

An SEM (HITACHI Regulus 8100, Japan) was used to observe the fracture surface morphology of PLA, PLA/*x*C composites, and PLA/*x*C@*y*B composites. To obtain brittle fracture surfaces, the samples were first immersed in liquid nitrogen for 2 h before inducing a rapid brittle fracture. Before SEM observation, the samples were baked in a vacuum oven at 40 °C for 6 h and then sprayed with gold.

2.6 Thermogravimetric analysis (TGA)

For TGA, the thermal decomposition of PLA, PLA/*x*C composites, and PLA/*x*C@*y*B composites were investigated using a Netzsch 209 F1 thermal analyzer (Germany). All measurements were heated from 25 to 600 °C at a rate of 10 °C/min under a nitrogen (N_2) atmosphere. The sample weight was about 5 mg.

2.7 Differential scanning calorimetry (DSC)

DSC analysis was performed using a Q2000 TA Instrument (Delaware, USA) under a nitrogen (N_2) atmosphere. Approximately 5 mg of the sample was placed in a sealed aluminum pan. To erase the thermal history of DSC, the temperature was increased from 25 to 200 °C at a rate of 10 °C/min followed by cooling to 25 °C at the same rate. Afterward, the second heating stage was performed under the same conditions as the first heating stage. Using DSC curves recorded in the second heating stage, the glass transition temperature (T_g), the cold crystallization temperature (T_{cc}), and the melting temperature (T_m) were determined. The degree of crystallinity (X_c) was calculated using Eq. (1):

$$Xc(\%) = \frac{\Delta Hm}{\Delta H \times wt\% \times 100} \tag{1}$$

where ΔHm represents the enthalpy of fusion of the composites, $\Delta H = 93.6\mathrm{J/g}$ represents the enthalpy of fusion when PLA is 100% crystallized, and $wt\%$ is the percentage of PLA in the composites [23].

2.8 Mechanical properties

Mechanical testing of PLA/*x*C@*y*B composites was performed using a universal mechanical testing instrument (Instron5966, USA). The Notched Izod impact strength was

tested using an XC-22 impact tester (Chengde, China). A total of 2-mm dumbbell-shaped spline was used for a tensile test and $80 \times 10 \times 4$ mm^3 rectangular-shaped samples were used for flexural and impact tests. The cross-head speeds for tensile and flexural tests were both 2 mm/min.

3 Results and discussion

3.1 Determination of CNTs content in PLA/*x*C/*y*B composites

Figure 2 shows the electrical conductivity change curves of PLA/*x*C composites with varying CNT contents. As the CNT content increases from 0 (PLA/0C) to 0.592 vol% (PLA/1C), the electrical conductivity of PLA/*x*C composites increases sharply and then stabilizes with a further increase in CNTs content. The percolation theory states that, in the process of filler dispersing in the polymer matrix, when the filler content reaches a level where it is able to bond together to form a conductive path, the conductivity begins to increase suddenly and will rise more than 10 orders of magnitude. The content of the filler is regarded as a critical value, which is called the percolation threshold [28]. Equation (2) is used to fit the electrical conductivity of the composites. [29–31]

$$\sigma = \sigma_0(\varphi - \varphi c)^t \tag{2}$$

where σ is the electrical conductivity of the sample, σ_0 is the electrical conductivity of CNTs, φ is the volume fraction of CNTs in the composites, φ_c is the percolation threshold, and t is the critical exponent.

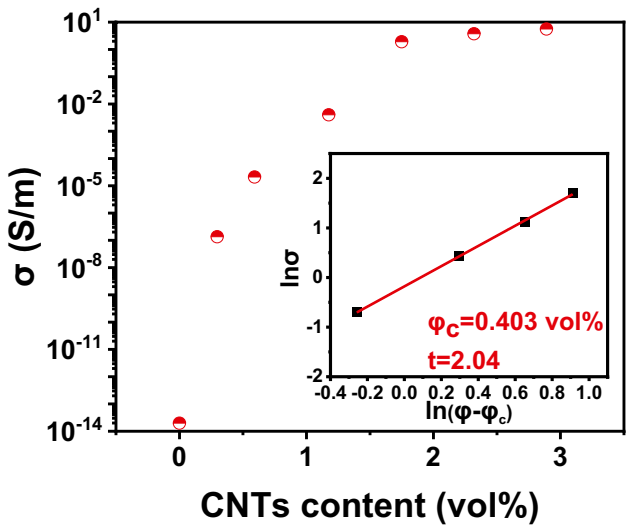

Fig. 2 Variation of electrical conductivity of PLA/*x*C composites with increasing CNTs content and the log–log plots of the electrical conductivity versus CNTs content of the composites

Analysis of the fitting results showed that the percolation threshold for PLA/*x*C composites was 0.403 vol% (the mass fraction of CNTs of about 0.7 wt%). When the filler content reaches the percolation threshold, a complete conductive pathway is formed within the composite. To maintain a good conductive pathway in composites, the CNT content should be increased to above 0.7 wt%.

Rheological tests were conducted on the composites to determine their rheological behavior [32]. The results shown in Fig. 3a demonstrate that, at low frequencies, the storage modulus (G') increases concomitantly with the increase in CNTs content. Higher CNTs content in the composite intensifies molecular entanglement, slows down polymer relaxation, and increases G'. An intensive molecular entanglement in a composites would slow down the flow of the melt, thereby increase the viscosity of the composites. As the viscous flow consumes more energy, the loss modulus (G'') increases (Fig. 3b). Additionally, rheological testing demonstrates that, when a filler forms a percolation network in the composites, the elastic response of the melt increases substantially, and the dependence of the elastic response on the shear frequency decreases significantly. As a result, the melt displays a solid-like behavior, which usually forms a plateau in G' and G'' curves at low frequencies [33]. Furthermore, in the low-frequency region, tan δ gradually decreases to below 1 as the CNTs content increases (Fig. 3c), indicating the gradual formation of the filler network and the liquid–solid transition of the melt [34]. The processing ability of the composites was further determined based on their complex viscosity (η^*). As shown in Fig. 3d, Newtonian behavior can be observed in the high frequency end region of PLA and PLA/0.5C composites. In contrast, other PLA/*x*C composites exhibit a strong tendency for shear thinning as the frequency is increased. This difference is caused by the gradual formation of the filler network, which limits the flow of the PLA matrix as the CNTs content increases. Furthermore, all composites exhibit lower viscosities at higher frequencies, implying better processing performance.

The brittle fracture surface morphology of the PLA/*x*C composites is shown in Fig. 4. Pure PLA in Fig. 4a exhibits typical brittle fracture characteristics [35, 36]. Conversely, as shown in Figs. 4b–g, the amount of CNTs on the fracture surface of the composites increase with an increase in CNT content. In contrast, significant agglomeration is observed on the fracture surface of composites when the CNTs content exceeds 3 wt% (Figs. 4e, f and g). On the basis of these results, PLA/1C and PLA/2C composites were selected as masterbatches for further investigation to maintain good conductive networks and prevent CNT agglomeration.

3.2 Morphology and properties of PLA/*x*C@*y*B composites

The comprehensive performance of polymer composites with segregated structures depends not only on filler

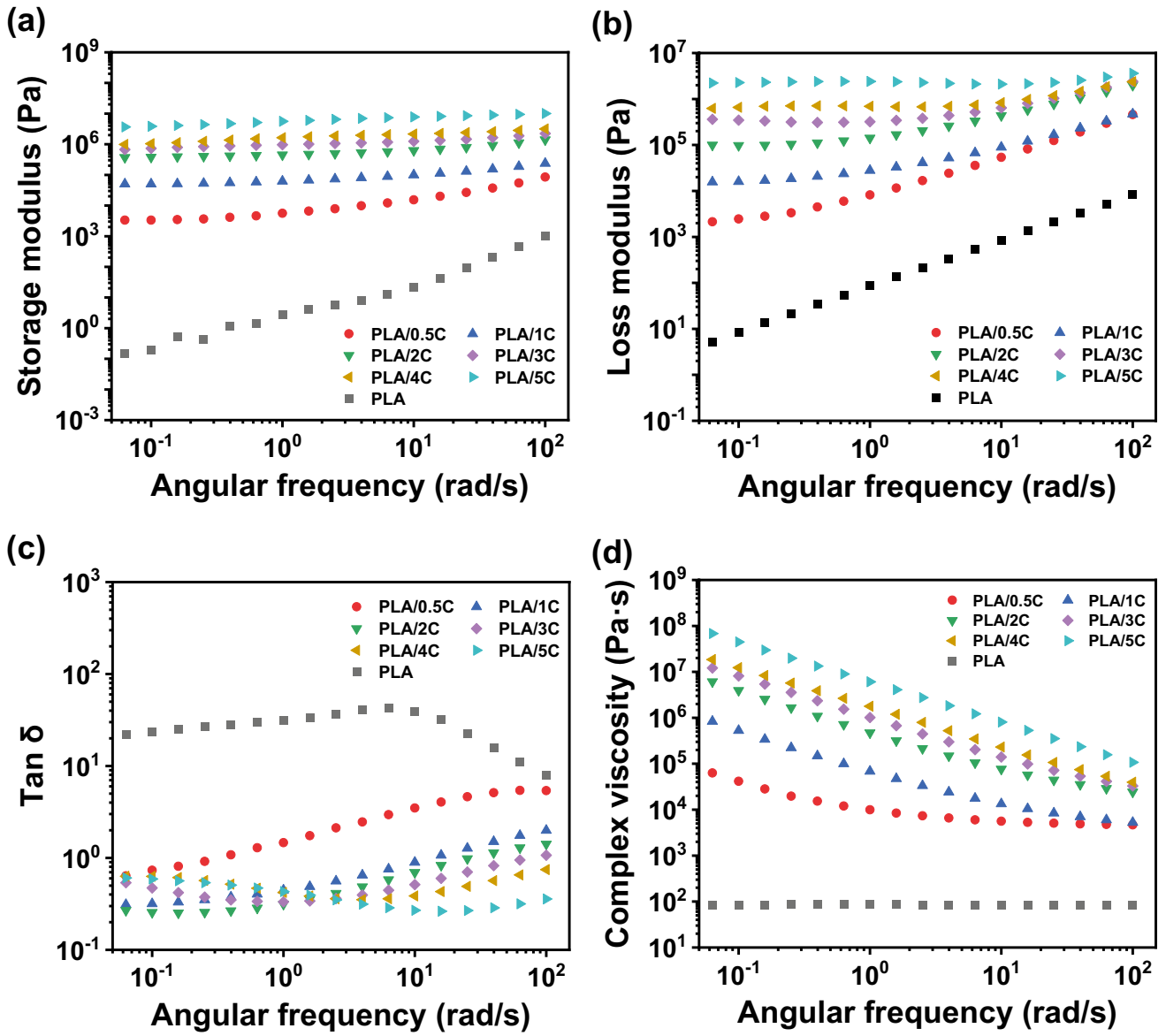

Fig. 3 Rheological properties of PLA/*x*C composites: (**a**) storage modulus (G'), (**b**) loss modulus (G''), (**c**) tan δ, and (**d**) complex viscosity (η^*)

dispersion and concentration but also on particle size [37]. Lei et al. [38] prepared PVDF/GNP conductive composites with segregated structures by mixing PVDF particles ranging in size from 100 to 400 μm with GNP and found that samples prepared with smaller PVDF particles formed a more dense conductive network. Another study by Gao et al. [39] compounded GPPS particles of various different sizes with graphite flakes to prepare composites with a segregated structure. They observed that the mechanical properties of the composites decreased with the increase in GPPS particle size. Likewise, Fig. 5 displays the surface morphology and size distribution of PLA/1C powder (Fig. 5a, b) and PLA/2C powder (Fig. 5c, d). PLA/1C powder and PLA/2C powder with a size less than 200 μm are very similar and have little effect on the subsequent experiment. Therefore, to improve the composites' electrical conductivity without compromising their mechanical properties, we sieved PLA/1C and PLA/2C composites to obtain PLA/*x*C powder masterbatches with sizes smaller than 200 μm.

After determining the particle sizes of PLA/1C and PLA/2C masterbatches, they were mechanically mixed with various CB contents to obtain PLA/*x*C/*y*B composites. The brittle fracture surfaces of PLA/1C/*y*B and PLA/2C/*y*B composites are shown in Fig. 6 and Fig. S1. As shown in Fig. 6a, the PLA/1C@1B composite can form a stable segregated network structure when a CB of 1 *phr* is added to the PLA/1C masterbatch. According to Fig. 6b–d, it is observed that the integrity of the conductive segregated

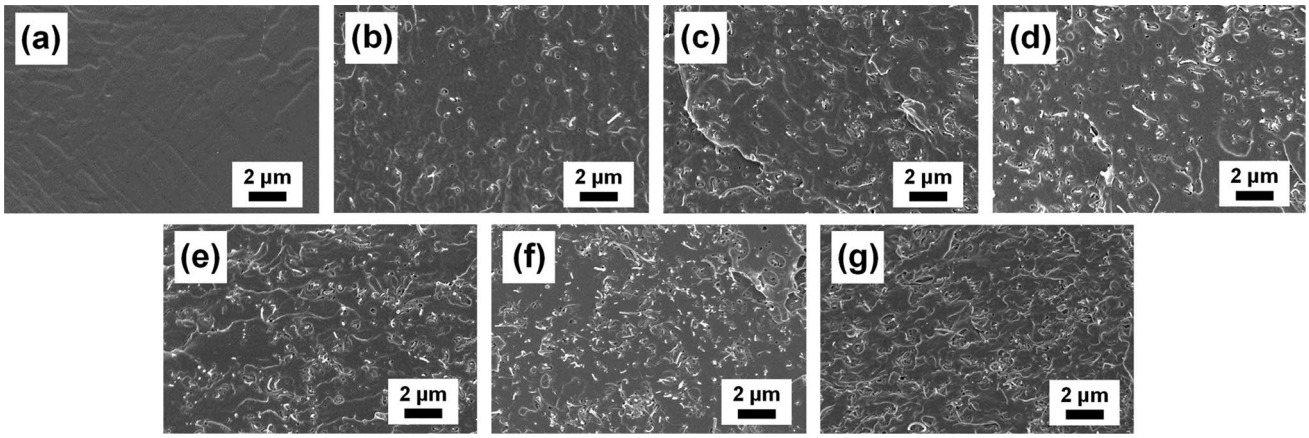

Fig. 4 SEM images of PLA/*x*C composites: (**a**) PLA, (**b**) PLA/0.5C, (**c**) PLA/1C, (**d**) PLA/2C, (**e**) PLA/3C, (**f**) PLA/4C, and (**g**) PLA/5C

network of the composites improves with the increase in CB content, and the width of the segregated zone increases with the increase in CB content, as can be seen from Fig. 6a_1–d_1. While the increase in CB content may contribute to improving the electrical conductivity of the sample, the overall structure of the polymer has not changed significantly. As a result, the electrical conductivity of the sample has not increased significantly. The morphology of PLA/2C/*y*B composites shown in Fig. S1 is similar to that of PLA/1C/*y*B composites. In addition, it can be clearly seen that, with increasing CB content, the segregated conductive network improves, and the width of the segregated zone increases, leading to higher electrical conductivity. Detailed results of electrical conductivity is provided in the following section.

TGA was used to evaluate the thermal stability of PLA and PLA/*x*C@*y*B composites under nitrogen (N_2) atmosphere [23]. The TGA and DTG curves are shown in Fig. 7 and the corresponding onset decomposition temperature (T_5), maximum weight loss temperature (DTG peak), and residual

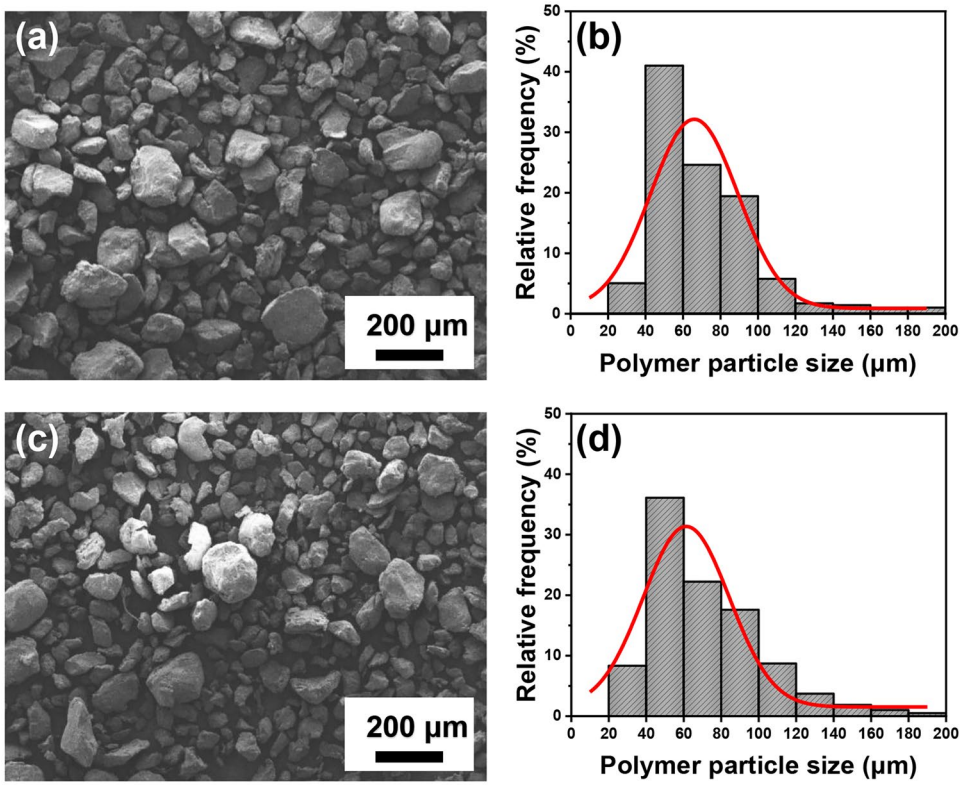

Fig. 5 SEM images and particle size distribution of (**a**, **b**) PLA/1C powder, (**c**, **d**) PLA/2C powder

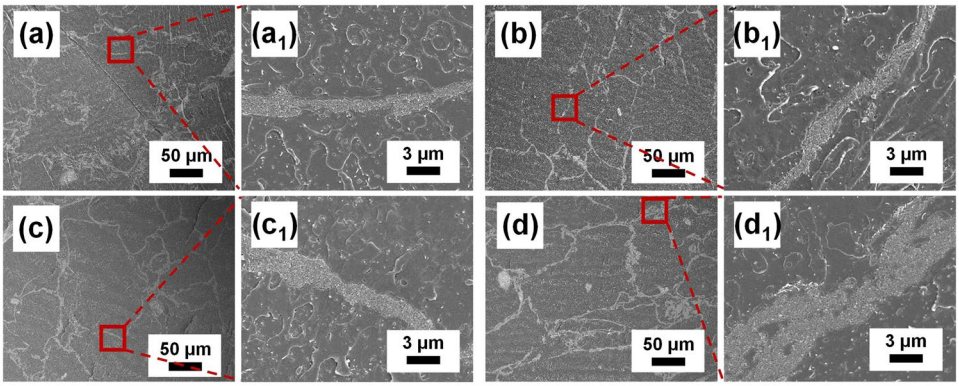

Fig. 6 SEM micrographs of PLA/1C@*y*B composites: (**a**, **a**$_1$) PLA/1C@1B, (**b**, **b**$_1$) PLA/1C@2B, (**c**, **c**$_1$) PLA/1C@3B, and (**d**, **d**$_1$) PLA/1C@4B

char mass are listed in Table S1. Based on the residual char mass, the actual content of the filler of the composite material is consistent with the theoretical content. As shown in Figs. 7c, d and Table S1, the initial decomposition temperature of PLA/1C@1B is 339.5 °C, and the maximum weight loss temperature is 371.4 °C, which is an increase of 2.4 °C and 2.1 °C over pure PLA, respectively, and an increase of 0.3 °C and 1.0 °C over PLA/1C. And the initial decomposition temperature and maximum weight loss temperature increase with increasing CB and CNTs content. At high CB and CNTs content, the thermal conductivity of the matrix is enhanced, thus improving PLA/*x*C@*y*B composites' thermal stability. According to these findings, adding CB and CNTs to composites improves their thermal stability and extends their service lives.

The effect of 0D CB-1D CNTs hybrid fillers on the crystallization properties of PLA nanocomposites is further investigated using DSC. A second heating curve can be seen in Fig. 8, and the composites' T_{cc}, T_m, ΔH_{cc}, ΔH_m, and X_c are listed in Table S2. Compared with pure PLA, PLA/*x*C@*y*B composites have a slightly higher T_g, since the CNTs and CBs inhibit the free movement of PLA chain segments. Notably, the T_{cc} of PLA composites is lower than that of pure PLA. This is caused by the heterogeneous nucleation role of CNTs and CB, which lowers the nucleation barrier and allowing

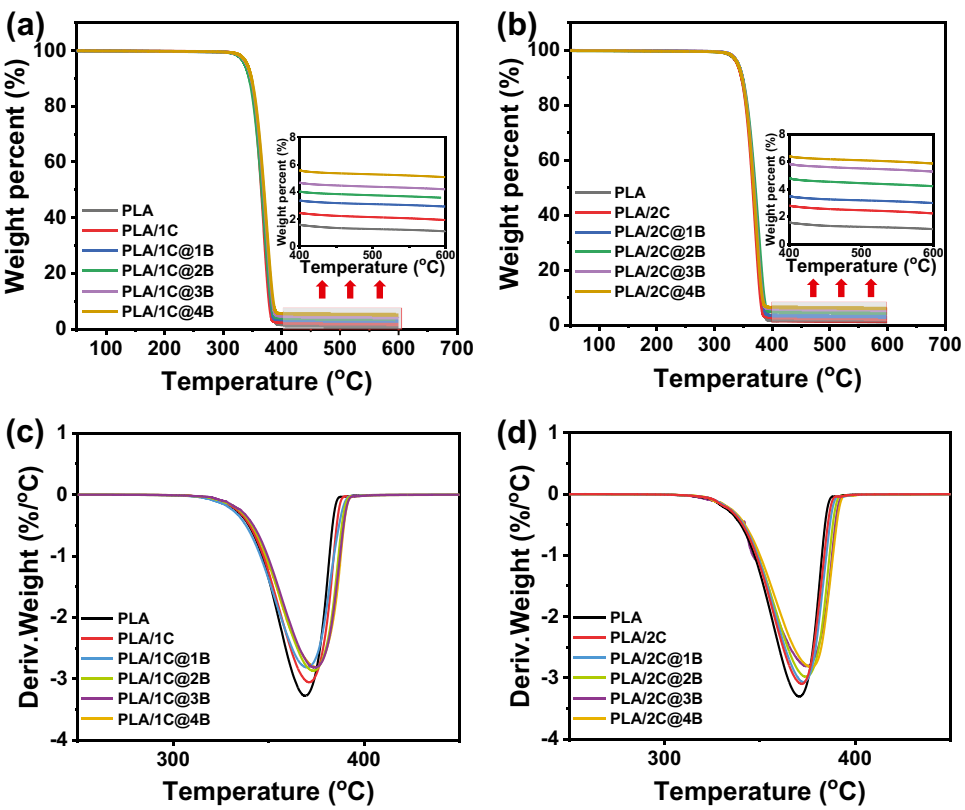

Fig. 7 TGA (**a**, **b**) and DTG (**c**, **d**) curves of pure PLA, PLA/*x*C composites and PLA/*x*C@*y*B composites

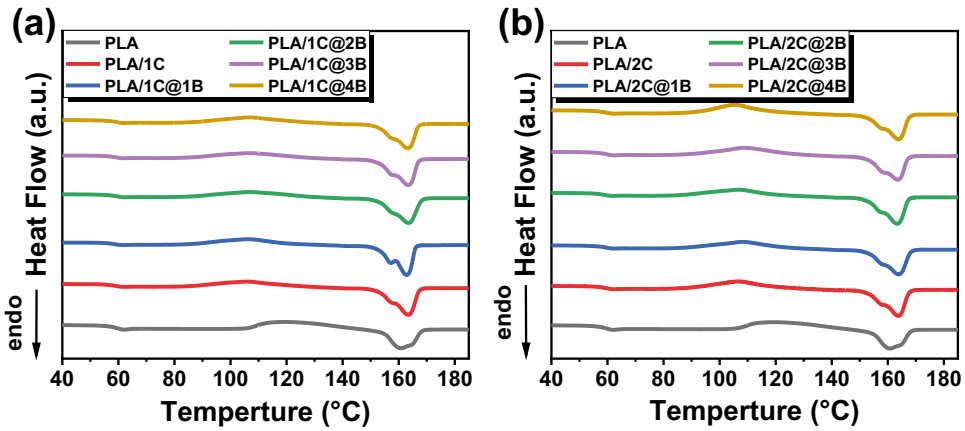

Fig. 8 The second heating curves of pure PLA and PLA/*x*C@*y*B composites

molecular chain segments to crystallize at lower temperatures. In addition, the crystallinity of PLA/*x*C@*y*B composites is significantly higher than that of pure PLA due to the heterogeneous nucleation effect of the hybrid nanofillers. PLA, for example, has a lower crystallinity of about 3.5% because of its slow crystallization and formation of crystals by cold crystallization during the second heating process. In contrast, the addition of CNTs and CB reduces the ΔH_{cc} and increases the melting enthalpy, leading to higher crystallinity. In PLA/2C@4B composites, the crystallinity is 18.5%, which is 5.3 times greater than that of pure PLA. Furthermore, the degree of crystal perfection is improved by adding CNTs and CB fillers, leading to an increase in T_m.

The mechanical properties of pure PLA and PLA/*x*C@*y*B composites are presented in Fig. 9. In comparison with the 3D-printed pure PLA sample, it is evident that all PLA/*x*C@*y*B composites have a higher tensile strength [40, 41]. A small amount of CNTs added to PLA could enhance its tensile strength. As a result of their reinforcing effect and good dispersion, PLA/1C composite (71.4 MPa) and PLA/2C composite (70.1 MPa) have higher tensile strength than PLA (68.6 MPa). By covering PLA/*x*C particles with CB, the tensile strength of PLA/*x*C@*y*B composites is decreased. For instance, PLA/1C@1B composite (70.1 MPa) has a lower tensile strength than PLA/1C composite (71.4 MPa). When PLA/*x*C particles are covered with a higher CB filler

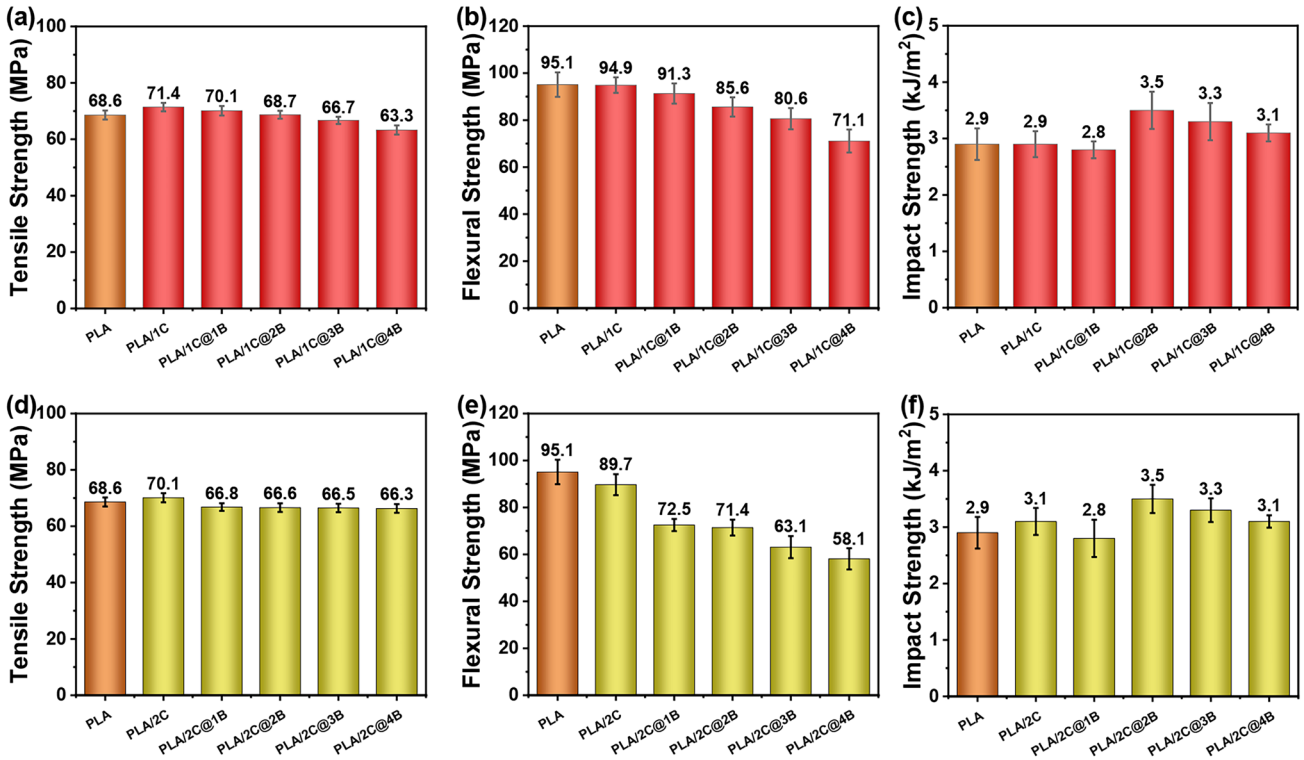

Fig. 9 Mechanical properties of pure PLA and PLA/*x*C@*y*B composites: (**a**, **d**) tensile strength, (**b**, **e**) flexural strength, and (**c**, **f**) impact strength

content, the decrease in tensile strength is more significant. Accordingly, the tensile strengths of PLA/1C@1B composite, PLA/1C@2B composite, PLA/1C@3B composite, and PLA/1C@4B composite are 70.1 MPa, 68.7 MPa, 66.7 MPa, and 63.3 MPa, respectively. Possibly, this inverse relationship can be attributed to the mechanical bonding between the CB fillers and the PLA/*x*C particles, which inhibits their interfacial adhesion. However, PLA/1C@4B composite has only a slight decrease in tensile strength with respect to PLA. Likewise, as the CB content increases in PLA/*x*C@*y*B composites, the composites' flexural strength gradually decreases (Fig. 9b, e). As compared to the flexural strength of PLA (95.1 MPa), the flexural strength of PLA1C/1B composite (91.3 MPa) is only reduced by approximately 4%. Figure 9c, f illustrates that there were no significant differences in impact strength between PLA and PLA/*x*C@*y*B composites. The PLA/1C/1B compositekJ/m has a similar impact strength (2.8 kJ/m^2) to pure PLA (2.9 kJ/m^2). To summarize, the addition of CNTs and CB does not significantly alter PLA's mechanical properties. The prepared composites are still able to maintain the high mechanical properties needed for most applications.

The electrical conductivity of pure PLA is 2.0×10^{-14} S/m, which is typical for insulating material, as illustrated in Fig. 10. After CNTs were added to PLA/*x*C composites, the electrical conductivity increased rapidly with increasing CNTs content. For example, the electrical conductivity of PLA/1C and PLA/2C was 2.9×10^{-4} S/m and 4.0×10^{-2} S/m, respectively, 10 and 12 times higher than that of pure PLA. This suggests that CNTs with good conductivity form a better conductive network with a uniform distribution in the PLA matrix. The electrical conductivity of PLA/*x*C@*y*B composites was further improved by mechanically coating the surface of PLA/*x*C particles with CB. The electrical conductivity of PLA/1C@1B composites and PLA/2C@1B composites was 9.8×10^{-2} S/m and 9.7×10^{-1} S/m, respectively, which was more than 12 and 13 times higher than that of pure PLA. It is worth noting that, at CB content exceeding 1 *phr*, increasing the CB content does not significantly enhance the electrical conductivity of PLA/*x*C@*y*B composites. These results demonstrate that 1 *phr* of CB is adequate to form a complete conductive network on the surface of PLA/*x*C particles. Mechanically coating 0D CB filler on the surface of the PLA/*x*C particles can improve the conductive network and connect far-apart CNTs on the surface of the particles, thus shortening the spacing of the conductive fillers and improving their connectivity. Therefore, we conclude that the high electrical conductivity of PLA/*x*C@*y*B composites at a low filler content is due to the formation of a segregated double-conductive network in the composite by the well-dispersed CNTs and the CB on the particle surface. Figure 10c shows the schematic diagram of the segregated double-filler network inside the PLA/*x*C@*y*B composite. In the PLA/*x*C composite masterbatch, the 0D CB filler forms a segregated

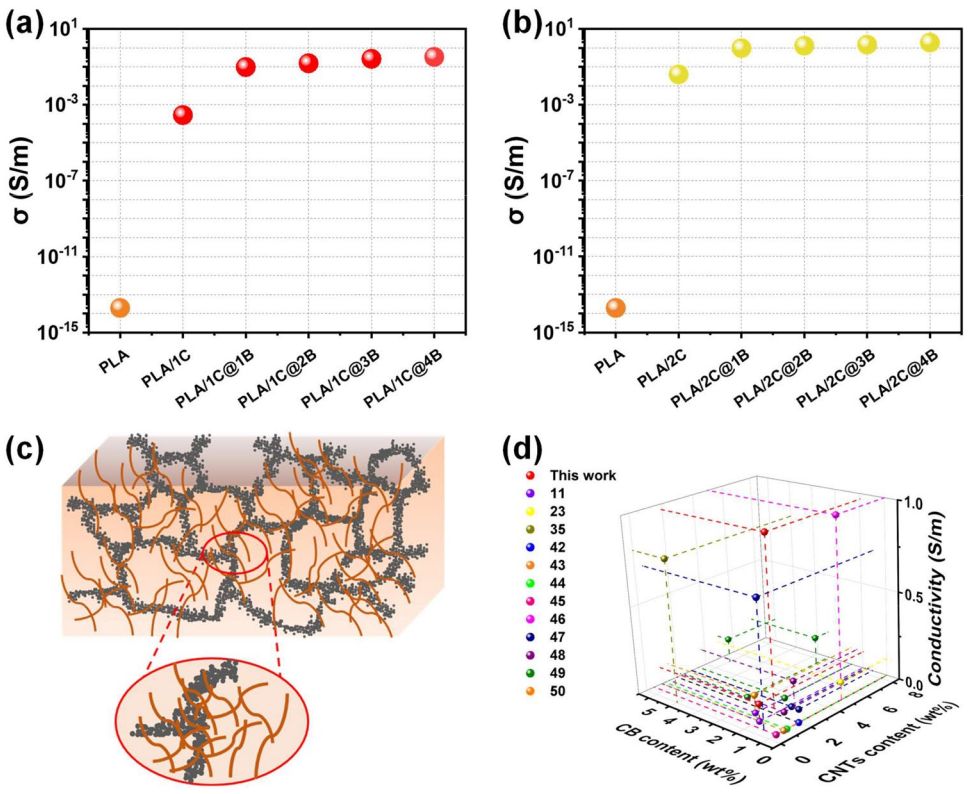

Fig. 10 Electrical conductivity of pure PLA and PLA/*x*C@*y*B composites (**a**, **b**), a schematic diagram of the segregated double-conductive network in PLA/*x*C@*y*B composites (**c**) and comparison of electrical conductivity with other previous works (**d**)

structure by enveloping composite particles and lapping with the CNTs with high aspect ratios to create more and better conductive paths. Thus, high electrical conductivity can be achieved in the PLA/*x*C@*y*B composites at low-hybrid nanofiller loadings. Figure 10d compares the electrical conductivity of PLA/1C@1B and PLA/2C@1B composites prepared in this study to that of PLA-based composites containing different conductive fillers reported previously. [11, 23, 35, 42–50] The results show that the composites prepared in this work can achieve relatively high electrical conductivity with low-filler contents, primarily because they contain successfully constructed segregated double-filler conductive networks.

4 Conclusions

In this study, PLA and 1D CNT fillers were melt-blended and sieved to obtain masterbatches with a size less than 200 μm. The obtained masterbatches were mechanically mixed with 0D CB filler. Finally, a segregated double-filler network structure was constructed in the PLA composites at low hybrid filler content. This structure increased the electrical conductivity of the composites. For example, the electrical conductivity of the PLA/1C@1B composite was more than 12 times higher than that of pure PLA with the addition of only 1 *phr* CNTs and 1 *phr* CB. The lower amount of filler can prevent filler agglomeration, which can also contribute to the maintenance of the composite's mechanical properties. The prepared PLA/1C@1B composites had tensile strength, flexural strength, and impact toughness of 70.1 MPa, 91.3 MPa, and 2.8 kJ/m^2, respectively, which is as good as pure PLA. Owing to the segregated double-filler conductive network, the PLA-based composites showed high electrical conductivity, good mechanical properties, and low preparation cost, making them ideal for application as electronic components and safety protection in the future.

Supplementary Information The online version contains supplementary material available at https://doi.org/10.1007/s42114-022-00622-z.

Author contribution T. R. Kuang, M. L. Zhang, B. Z. Wu, and T. Liu wrote the main manuscript text; F. Chen, Y. P. Fei, J. T. Yang, M. Q. Zhong, and B. Z. Wu provided pieces of advice and suggestions; T. R. Kuang, M. L. Zhang, and T. Liu prepared Figs. 1, 2, 3, 4, 5, 6, 7, 8, 9, and 10. All the authors reviewed the manuscript.

Funding This work was financially supported by the National Natural Science Foundation of China (Nos. 51873193, 51803062, 52173046, and 52173086) and Natural Science Foundation of Zhejiang Province (No. LZ21E030002).

Declarations

Conflict of interest The authors declare no competing interests.

References

1. Tansel B (2017) From electronic consumer products to e-wastes: Global outlook, waste quantities, recycling challenges. Environ Int 98:35–45
2. Kuang T, Ju J, Liu T, Hejna A, Saeb MR, Zhang S, Peng X (2022) A facile structural manipulation strategy to prepare ultra-strong, super-tough, and thermally stable polylactide/nucleating agent composites. Adv Compos Hybrid Mater 5(2):948–959
3. Kuang T, Ju J, Chen F, Liu X, Zhang S, Liu T, Peng X (2022) Coupled effect of self-assembled nucleating agent, Ni-CNTs and pressure-driven flow on the electrical, electromagnetic interference shielding and thermal conductive properties of poly (lactic acid) composite foams. Compos Sci Technol 230:109736
4. Chen Y, Lin J, Mersal GAM, Zuo JL, Li JL, Wang QY, Feng YH, Liu JW, Liu ZL, Wang B, Xu BB, Guo ZH (2022) "Several birds with one stone" strategy of pH/thermoresponsive flame-retardant/photothermal bactericidal oil-absorbing material for recovering complex spilled oil. J Mater Sci Technol 128:82–97
5. Pan D, Yang G, Abo-Dief HM, Dong JW, Su FM, Liu CT, Li YF, Xu BB, Murugadoss V, Naik N, El-Bahy SM, El-Bahy ZM, Huang MA, Guo ZH (2022) Vertically aligned silicon carbide nanowires/boron nitride cellulose aerogel networks enhanced thermal conductivity and electromagnetic absorbing of epoxy composites. Nano-Micro Lett 14(1):118
6. Ju J, Peng X, Huang K, Li L, Liu X, Chitrakar C, Chang L, Gu Z, Kuang T (2019) High-performance porous PLLA-based scaffolds for bone tissue engineering: Preparation, characterization, and in vitro and in vivo evaluation. Polymer 180:121707
7. Liu T, Lian X, Li L, Peng X, Kuang T (2020) Facile fabrication of fully biodegradable and biorenewable poly (lactic acid)/poly (butylene adipate-co-terephthalate) in-situ nanofibrillar composites with high strength, good toughness and excellent heat resistance. Polym Degrad Stab 171:109044
8. Kuang TR, Zhang JB, Chen F, Fei YP, Zhou HF, Weng YX, Liu T, Yang JT, Zhong MQ (2022) A simple, low-cost, and green method for preparing strong, tough, and ductile poly(lactic acid) materials with good transparency and heat resistance. Acs Sustain Chem Eng 10:16389–16398
9. Wang Z, Liu T, Yang JT, Chen F, Fei YP, Zhong MQ, Kuang TR (2022) Biomimetically structured poly(lactic acid)/poly(butylene-adipate-co-terephthalate) blends with ultrahigh strength and toughness for structural application. Acs Appl Polym Mater 4:9351–9359
10. Wen X, Liu Z, Li Z, Zhang J, Wang D-Y, Szymańska K, Chen X, Mijowska E, Tang T (2020) Constructing multifunctional nanofiller with reactive interface in PLA/CB-g-DOPO composites for simultaneously improving flame retardancy, electrical conductivity and mechanical properties. Compos Sci Technol 188:107988
11. Wu D, Lv Q, Feng S, Chen J, Chen Y, Qiu Y, Yao X (2015) Polylactide composite foams containing carbon nanotubes and carbon black: Synergistic effect of filler on electrical conductivity. Carbon 95:380–387
12. Kuan C-F, Kuan H-C, Ma C-CM, Chen C-H (2008) Mechanical and electrical properties of multi-wall carbon nanotube/poly(lactic acid) composites. J Phys Chem Solids 69(5):1395–1398
13. Cui C-H, Yan D-X, Pang H, Xu X, Jia L-C, Li Z-M (2016) Formation of a segregated electrically conductive network structure in a low-melt-viscosity polymer for highly efficient electromagnetic interference shielding. ACS Sustain Chem Eng 4(8):4137–4145
14. Wang Y, Yang C, Xin Z, Luo Y, Wang B, Feng X, Mao Z, Sui X (2022) Poly (lactic acid)/carbon nanotube composites with enhanced electrical conductivity via a two-step dispersion strategy. Compos Commun 30:101087

15. Yu B, Zhao Z, Fu S, Meng L, Liu Y, Chen F, Wang K, Fu Q (2019) Fabrication of /CNC/CNT conductive composites for high electromagnetic interference shielding based on Pickering emulsions method. Compos Part A-Appl Sci 125:105558
16. Wang Z, Zhu HB, Cao N, Du RK, Liu YQ, Zhao GZ (2017) Superhydrophobic surfaces with excellent abrasion resistance based on benzoxazine/mesoporous SiO2. Mater Lett 186:274–278
17. Li XY, Zhao SP, Hu WH, Zhang X, Pei L, Wang Z (2019) Robust superhydrophobic surface with excellent adhesive properties based on benzoxazine/epoxy/mesoporous SiO2. Appl Surf Sci 481:374–378
18. Hu WH, Huang JG, Zhang X, Zhao SP, Pei L, Zhang CY, Liu YQ, Wang Z (2020) A mechanically robust and reversibly wettable benzoxazine/epoxy/mesoporous TiO2 coating for oil/water separation. Appl Surf Sci 507:145168
19. Deng H, Lin L, Ji M, Zhang S, Yang M, Fu Q (2014) Progress on the morphological control of conductive network in conductive polymer composites and the use as electroactive multifunctional materials. Prog Polym Sci 39(4):627–655
20. Wang M, Tang X-H, Cai J-H, Wu H, Shen J-B, Guo S-Y (2021) Construction, mechanism and prospective of conductive polymer composites with multiple interfaces for electromagnetic interference shielding: A review. Carbon 177:377–402
21. Yao FC, Xie WH, Ma C, Wang DD, El-Bahy ZM, Helal MH, Liu H, Du A, Guo ZH, Gu HB (2022) Superb electromagnetic shielding polymer nanocomposites filled with 3-dimensional p-phenylenediamine/aniline copolymer nanofibers@copper foam hybrid nanofillers. Compos Part B-Eng 245:110236
22. Ren F, Li Z, Xu L, Sun Z, Ren P, Yan D, Li Z (2018) Large-scale preparation of segregated PLA/carbon nanotube composite with high efficient electromagnetic interference shielding and favourable mechanical properties. Compos Part B-Eng 155:405–413
23. Guo J, Tsou C-H, Yu Y, Wu C-S, Zhang X, Chen Z, Yang T, Ge F, Liu P, Guzman MRD (2021) Conductivity and mechanical properties of carbon black-reinforced poly(lactic acid) (PLA/CB) composites. Iran Polym J 30(12):1251–1262
24. Kashi S, Gupta RK, Baum T, Kao N, Bhattacharya SN (2016) Morphology, electromagnetic properties and electromagnetic interference shielding performance of poly lactide/graphene nanoplatelet nanocomposites. Mater Des 95:119–126
25. Wang Y, Wang P, Du Z, Liu C, Shen C, Wang Y (2022) Electromagnetic interference shielding enhancement of poly (lactic acid)-based carbonaceous nanocomposites by poly (ethylene oxide)-assisted segregated structure: a comparative study of carbon nanotubes and graphene nanoplatelets. Adv Compos Hybrid Mater 5(1):209–219
26. Urquijo J, Aranburu N, Dagréou S, Guerrica-Echevarría G, Eguiazábal J (2017) CNT-induced morphology and its effect on properties in PLA/PBAT-based nanocomposites. Eur Polym J 93:545–555
27. Zhu QS, Zhao Y, Miao BJ, Abo-Dief HM, Qu MC, Pashameah RA, Bin XuB, Huang MA, Algadi H, Liu XH, Guo ZH (2022) Hydrothermally synthesized ZnO-RGO-PPy for water-borne epoxy nanocomposite coating with anticorrosive reinforcement. Prog Org Coat 172:107153
28. Luo Y, Xiong SY, Zhang F, He XX, Lu X, Peng RT (2021) Preparation of conductive polylactic acid/high density polyethylene/carbon black composites with low percolation threshold by locating the carbon black at the Interface of co-continuous blends. J Appl Polym Sci 138(17):50291
29. Potschke P, Bhattacharyya AR, Janke A (2004) Carbon nanotube-filled polycarbonate composites produced by melt mixing and their use in blends with polyethylene. Carbon 42(5–6):965–969
30. Kuang T, Chang L, Chen F, Sheng Y, Fu D, Peng X (2016) Facile preparation of lightweight high-strength biodegradable polymer/multi-walled carbon nanotubes nanocomposite foams for electromagnetic interference shielding. Carbon 105:305–313
31. Ju J, Kuang T, Ke X, Zeng M, Chen Z, Zhang S, Peng X (2020) Lightweight multifunctional polypropylene/carbon nanotubes/carbon black nanocomposite foams with segregated structure, ultralow percolation threshold and enhanced electromagnetic interference shielding performance. Compos Sci Technol 193:108116
32. Lu Y, Sun DX, Qi XD, Lei YZ, Yang JH, Wang Y (2020) Achieving ultrahigh synergistic effect in enhancing conductive properties of polymer composites through constructing the hybrid network of "rigid" submicron vapor grown carbon fibers and "reelable" carbon nanotubes. Compos Sci Technol 193:108141
33. Bai QQ, Jin XZ, Yang JH, Qi XD, Wang Y (2019) Constructing network structure of graphene nanoplatelets/carbon nanofibers in polystyrene and the resultant heat resistance, thermal and conductive properties. Compos Part A-Appl Sci Manuf 117:299–307
34. Shi SH, Peng ZL, Jing JJ, Yang L, Chen YH, Kotsilkova R, Ivanov E (2020) Reparation of highly efficient electromagnetic interference shielding polylactic acid/graphene nanocomposites for fused deposition modeling three-dimensional printing. Ind Eng Chem Res 59(35):15565–15575
35. Wang LJ, Qiu JH, Sakai E, Wei XW (2016) The relationship between microstructure and mechanical properties of carbon nanotubes/polylactic acid nanocomposites prepared by twin-screw extrusion. Compos Part A-Appl Sci Manuf 89:18–25
36. Li Y, Yin DX, Liu W, Zhou HF, Zhang YX, Wang XD (2020) Fabrication of biodegradable poly (lactic acid)/carbon nanotube nanocomposite foams: significant improvement on rheological property and foamability. Int J Biol Macromol 163:1175–1186
37. Murariu M, Bonnaud L, Yoann P, Fontaine G, Bourbigot S, Dubois P (2010) New trends in polylactide (PLA)-based materials: "Green" PLA-Calcium sulfate (nano) composites tailored with flame retardant properties. Polym Degrad Stabil 95(3):374–381
38. Lei YZ, Bai Y, Shi Y, Liang M, Zou HW, Zhou ST (2022) Composite nanoarchitectonics of poly(vinylidene fluoride)/graphene for thermal and electrical conductivity enhancement via constructing segregated network structure. J Polym Res 29(5):213
39. Gao CW, Feng CP, Lu H, Ni HY, Chen J (2018) Thermally conductive general-purpose polystyrene (GPPS)/graphite composite with a segregated structure: effect of size of resin and graphite flakes. Polym-Plast Technol 57(13):1277–1287
40. Ecker JV, Haider A, Burzic I, Huber A, Eder G, Hild S (2019) Mechanical properties and water absorption behaviour of PLA and PLA/wood composites prepared by 3D printing and injection moulding. Rapid Prototyp J 25(4):672-678
41. Jayanth N, Jaswanthraj K, Sandeep S, Mallaya NH, Siddharth SR (2021) Effect of heat treatment on mechanical properties of 3D printed PLA. J Mech Behav Biomed 123:104764
42. Quan H, Zhang SJ, Qiao JL, Zhang LY (2012) The electrical properties and crystallization of stereocomplex poly(lactic acid) filled with carbon nanotubes. Polymer 53(20):4547–4552
43. Kobashi K, Villmow T, Andres T, Potschke P (2008) Liquid sensing of melt-processed poly(lactic acid)/multi-walled carbon nanotube composite films. Sensor Actuat B-Chem 134(2):787–795
44. Kim HS, Chae YS, Park BH, Yoon JS, Kang M, Jin HJ (2008) Thermal and electrical conductivity of poly(L-lactide)/multiwalled carbon nanotube nanocomposites. Curr Appl Phys 8(6):803–806
45. Zhang K, Peng JK, Shi YD, Chen YF, Zeng JB, Wang M (2016) Control of the crystalline morphology of poly(L-lactide) by addition of high-melting-point poly(L-lactide) and its effect on the distribution of multiwalled carbon nanotubes. J Phys Chem B 120(30):7423–7437
46. Zhang DG, Liu X, Wu GZ (2016) Forming CNT-guided stereocomplex networks in polylactide-based nanocomposites. Compos Sci Technol 128:8–16

47. Zhang ZX, Xiang D, Wu YP, Zhang J, Li YX, Wang MH, Li ZY, Zhao CX, Li H, Wang P, Li YT (2022) Effect of carbon black on the strain sensing property of 3D printed conductive polymer composites. Appl Compos Mater 29(3):1235–1248
48. Bertolini MC, Ramoa SDAS, Merlini C, Barra GMO, Soares BG, Pegoretti A (2020) Hybrid composites based on thermoplastic polyurethane with a mixture of carbon nanotubes and carbon black modified with polypyrrole for electromagnetic shielding. Front Mater 7:174.
49. Zhou ST, Hrymak AN, Kamal MR (2018) Effect of hybrid carbon fillers on the electrical and morphological properties of polystyrene nanocomposites in microinjection molding. Nanomaterials 8(10):779
50. Schmitz DP, Ecco LG, Dul S, Pereira ECL, Soares BG, Barra GMO, Pegoretti A (2018) Electromagnetic interference shielding effectiveness of ABS carbon-based composites manufactured via fused deposition modelling. Mater Today Commun 15:70–80